ACS Photonics

Letter

pubs.acs.org/journal/apchd5

Flexible Opto-Fluidic Fluorescence Sensors Based on Heterogeneously Integrated Micro-VCSELs and Silicon Photodiodes

Dongseok Kang,[†] Boju Gai,[†] Bryant Thompson,[‡] Sung-Min Lee,[†] Noah Malmstadt,[†,‡] and Jongseung Yoon*[,†,§]

Departments of [†]Chemical Engineering and Materials Science, [‡]Biomedical Engineering, and [§]Electrical Engineering, University of Southern California, Los Angeles, California 90089, United States

Supporting Information

ABSTRACT: We present mechanically flexible opto-fluidic fluorescence sensors based on heterogeneously integrated microscale vertical cavity surface emitting lasers (micro-VCSELs) and silicon photodiodes (Si-PDs). Micro- and millimeters-scale, printable forms of 850 nm-emitting micro-VCSELs and Si-PDs are coassembled into integrated fluorescence sensor arrays over large area in flexible, liquid-proof constructions on a polyethylene terephthalate (PET) substrate, where lithographically defined optical isolation trenches and multilayer-based wavelength- and angle-selective spectral filters are incorporated to effectively block the waveguided and reflected excitation light to the Si-PD and, thus, significantly enhance the signal-to-noise ratio and detection limit. The resulting optoelectronic fluorescence sensors integrated with elastomeric fluidic channels on plastics also enable mechanically bendable operation at a bending radius of down to ∼50 mm, as well as multiplexed, real-time monitoring of fluorescent analytes flown through the opto-fluidic channels, with minimum detectable luminophore concentration of 5×10^{-5} wt %.

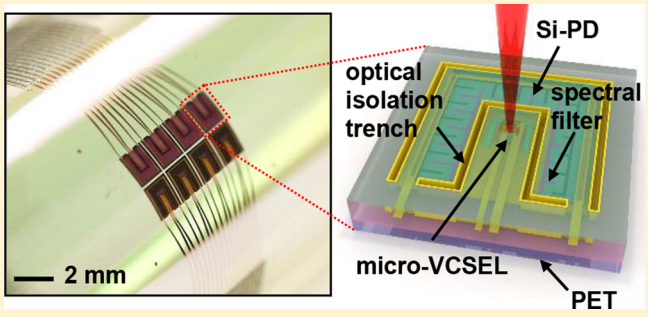

KEYWORDS: *VCSELs, fluorescence sensors, lasers, flexible electronics, transfer printing*

With increasing demands for monitoring infectious diseases or toxic chemicals in a fast and accurate manner, much research efforts have been devoted to developing compact, widely deployable diagnostic systems.[1−3] In particular, fluorescence-based sensing is one of the most powerful techniques that can provide both high sensitivity and high selectivity and, thus, an important candidate method for miniaturized, high-throughput screening and detection.[4,5] However, despite well-established procedures for high fidelity sensing, conventional fluorescence microscopy and spectroscopy often rely on benchtop or laboratory scale instruments, thereby limiting their applications in remote diagnostics and long-term monitoring of mobile subjects.[6] In this regard, solid-state optoelectronic systems based on vertical cavity surface emitting lasers (VCSELs) and semiconductor photodiodes (PDs) represent an alternative transducer platform that can readily accommodate thin, lightweight, and miniaturized form factors. VCSELs as a deep red (650−700 nm) or near-infrared (NIR, 750−1000 nm) light source can provide surface-normal, directional light output, circular and low divergence beam profile, narrow spectral bandwidth, as well as low power consumption, all of which constitute significant advantages in fluorescence sensing that translate into high spatial resolution, reduced interference, large spectral separation, and remote, low-cost operation.[7,8] Integrated VCSEL-based fluorescence sensors were first demonstrated by Thrush et al.[9,10] In this pioneering work, GaAs-based 773 nm VCSELs and GaAs photodiodes were grown monolithically on the same growth substrate, where the bottom n-type distributed Bragg reflector (DBR) and underlying intrinsic GaAs layer grown on a p-type GaAs substrate served as a filter-incorporated PIN photodiode.[9] The fabricated sensors were placed in a close proximity to a dye-coated glass substrate or a microfluidic channel filled with a dye solution to collect fluorescent signals. More recently, similar optoelectronic sensors using shorter-wavelength (675 nm) AlGaInP-based VCSELs were also reported for continuous monitoring of fluorescence from cyanine 5.5 dye in a mouse model with a maximum sensitivity of 50 nM.[11−14] Although configured well for many applications, such monolithically grown wafer-based sensor platforms fabricated by conventional semiconductor packaging schemes have limitations in the spatial layout and areal coverage of constituting devices, which therefore restrict the recording of fluorescence signals only at one or a few locations at a time and are not suited for spatiotemporal imaging over large subject areas. Moreover, the main system components (i.e., VCSEL and PD) are built on the rigid and brittle surface of a semiconductor wafer, thereby intrinsically limiting their conformal, harmonious integration onto soft, curvilinear surfaces such as those in biological

Received: February 2, 2016
Published: April 4, 2016

DOI: 10.1021/acsphotonics.6b00080
ACS Photonics 2016, 3, 912−918

systems. To address these challenges in the conventional VCSEL technology, we have previously reported printable forms of microscale VCSELs (micro-VCSELs) that can be released from the GaAs growth wafer and printed onto virtually any types of non-native substrates in programmable arrangements with no compromise in performance.[15,16] Building on these advances, we here report a type of large area, mechanically flexible optoelectronic fluorescence sensor formed on a thin sheet of plastics based on heterogeneously assembled micro-VCSELs and silicon photodiodes (Si-PDs) via printing-based deterministic materials assemblies.[17] The resulting integrated fluorescence sensors exhibited the enhanced signal-to-background ratio by rationally designed wavelength- and angle-selective spectral filters as well as metal-coated optical isolation trenches. Furthermore, liquid-proof construction of the device assemblies on a polyethylene terephthalate (PET) substrate in thermally and mechanically optimized constructions allowed their intimate integration with elastomeric fluidic channels made of polydimethylsiloxane (PDMS) to form thin, large area opto-fluidic sensor arrays capable of mechanically bendable sensing operations on curved surfaces at a bending radius of as small as 50 mm.

Figure 1a shows schematic illustrations of optoelectronic fluorescence sensors based on heterogeneously integrated micro-VCSELs and Si-PDs as a light source for excitation and a detector for fluorescence emission, respectively, on a non-native substrate such as silicon or plastics. A brief description of fabrication steps is provided below, with additional details available in the Supporting Information. Printable forms of 850 nm emitting micro-VCSELs with an aperture area of 22 × 22 μm^2 were prepared by previously reported procedures.[15,16] The C-shaped thin (~3 μm) p^+nn^+ single-crystalline Si-PDs were fabricated from a n-type (100) silicon-on-insulator (SOI) wafer (1−10 Ω·cm, Soitec), in which thermal diffusion of solid-state doping sources formed a pn-junction and heavily doped regions for making ohmic contacts, followed by photolithography and reactive-ion etching (RIE) to delineate isolated photodetector arrays with interdigitated doping layouts (see the inset of Figure 1b).[18,19] Independently fabricated micro-VCSELs and silicon PDs were released from respective source wafers by selective wet chemical etching of sacrificial layers (i.e., AlAs for VCSEL and SiO_2 for Si-PD) and printed onto a target substrate using a thin (~1 μm) layer of photocurable adhesive in a predefined layout such that the micro-VCSEL is positioned deterministically at the center of the C-shaped Si-PD (Figure 1b), in which procedures of transfer printing provided a fast, cost-effective means to the integration of heterogeneous collections of devices without limitations associated with the materials and processing compatibilities, device types, or the original size of source wafers.[17,20] Subsequently, metal interconnects were formed by electron beam evaporation and liftoff, followed by the encapsulation with a photopatternable epoxy (i.e., SU-8) in schemes that incorporate lithographically defined optical isolation trenches as well as angle- and wavelength-selective spectral filters to reduce optical cross-talks between the cointegrated micro-VCSELs and Si-PDs. The fabrication of the flexible fluorescence sensor arrays were completed by forming external connections using anisotropic conductive film (ACF, Elform) for the electrical control and readout of individual devices. Figure 1c shows a photographic image of 2 × 4 arrays of completed VCSEL-based fluorescence sensors integrated on a PET substrate, mounted on a cylindrical support at a bending radius of 12 mm.

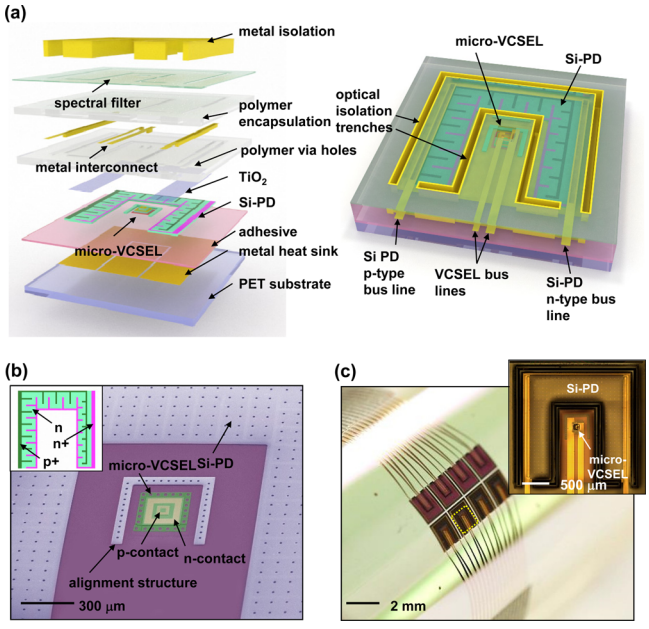

Figure 1. (a) Exploded- (left) and tilt-view (right) schematic illustrations of mechanically flexible integrated fluorescence sensors based on heterogeneously integrated micro-VCSELs and silicon photodiodes (Si-PDs) on a polyethylene terephthalate (PET) substrate. (b) Tilt-view colorized scanning electron microscope (SEM) image of an 850 nm-emitting micro-VCSEL cointegrated with a 3 μm-thick Si-PD on a silicon substrate. The inset shows the detailed doping layouts of Si-PD including n^+- and p^+-doped regions in the n-type background. (c) Photographic image of a 2 × 4 array of the interconnected fluorescence sensor on PET wrapped on a cylindrical support (bending radius: 12 mm). The inset shows a magnified view of an isolated sensor assembly.

The baseline device performance of printed micro-VCSELs and Si-PDs were first characterized before examining their performance of fluorescence sensing. Figure 2a shows optical output power (L)-current (I) curves of a micro-VCSEL printed on silicon at various stages of fabrication steps. The maximum output power (L_{max}) of the micro-VCSEL with an aperture area of 22 × 22 μm^2 decreased from ~4.5 mW on a GaAs source wafer to ~3.0 mW on a silicon substrate arising from the restricted heat dissipation associated with an order of magnitude low thermal conductivity of the polymeric adhesive.[21] The L_{max} slightly increased after the via formation and deposition of metal layers, possibly due to the evaporation of a residual solvent in the adhesive layer during the thermal curing and corresponding increase in thermal conductivity, which is also consistent with the decreased slope of wavelength shift for lasing modes (Figure S1). Notably, the output power of lasing substantially increased to the level (~5.3 mW) that is even higher than that on the GaAs source wafer after the additional polymer encapsulation, which is attributed to the coverage of the polymer (i.e., SU-8) layer on top of the laser aperture and resultant increase of the transmitted lasing output (Figure S2).[22]

One of important requirements for high sensitivity fluorescence sensing is to eliminate or reduce the contribution of excitation light source to the detector response, as it can be even higher than the fluorescence emission and therefore deteriorate the signal-to-noise ratio and detection limit. In the reported micro-VCSEL/Si-PD system, the spontaneously

DOI: 10.1021/acsphotonics.6b00080
ACS Photonics 2016, 3, 912−918

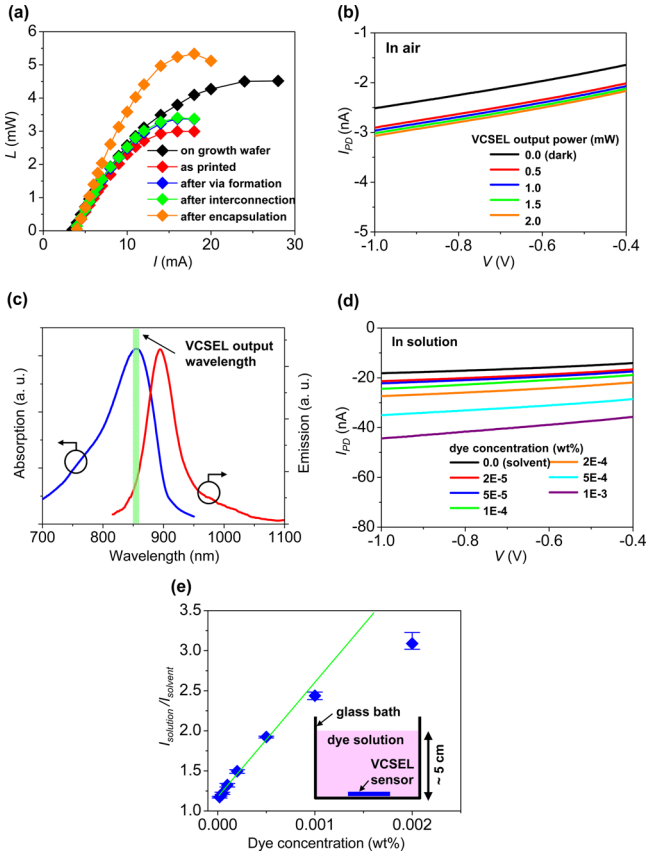

Figure 2. (a) Representative optical output power (L)-current (I) data collected from an 850 nm micro-VCSEL with a square aperture of 22 × 22 μm^2 at various fabrication stages including the device on a growth wafer (black); after the printing on a silicon substrate (red); after the via formation (blue); after the metal deposition for interconnects (green); after the encapsulation with SU-8 (orange). (b) Current (I)-voltage (V) curves of a printed Si-PD on silicon at various output power levels of the cointegrated micro-VCSEL, measured in air after the implementation of optical isolation trenches. (c) Absorbance and emission spectra of an infrared-absorbing organic dye (IR 143, Exciton) dissolved in the mixture of dimethyl sulfoxide (DMSO) and ethylene glycol (EG) (DMSO/EG = 1:2 by weight) at the concentration of 5 × 10^{-4} wt % (6.75 μM). The emission spectra were obtained at the excitation wavelength of 750 nm. (d) IV curves of a Si-PD printed on silicon measured at various dye concentrations under a fixed output power (~2 mW) of the micro-VCSEL, where the integrated fluorescence sensor is immersed in a bath containing a dye solution. (e) Corresponding background-normalized current ($I_{solution}/I_{solvent}$) of the Si-PD at a fixed bias (i.e., −1.0 V) as a function of dye concentration. The output optical power of the micro-VCSEL was fixed at 2.0 mW.

emitted light from the sidewall of the micro-VCSEL can be wave-guided through a polymeric medium to the adjacent Si-PD, resulting in the false increase of the PD current even without the presence of fluorescent signals (Figure S3). To reduce such undesired optical "cross-talks" between the excitation source and the detector, we first introduced a metal-coated trench structure in the surrounding region of the printed Si-PD by photolithography and metal deposition to block the wave-guided photon flux from the VCSEL to the Si-PD (Figures 1a and S4). Figure 2b shows current (I)-voltage (V) curves of a Si-PD printed on silicon at various output power levels (0−2.0 mW) of the cointegrated micro-VCSEL, measured after the implementation of optical isolation channels in an ambient condition (i.e., air, without luminophores). The variation of PD current between "OFF" and "ON" states of the micro-VCSEL is significantly smaller (<~1 nA) than that (~35 μA) obtained from samples without the isolation scheme (Figure S3) owing to the effective blocking of the wave-guided excitation source. As fluorescent analytes, we employed an infrared-absorbing organic dye (IR 143, Exciton) dissolved in the mixture of dimethyl sulfoxide (DMSO) and ethylene glycol (EG) (DMSO/EG = 1:2 by weight). The peak wavelength (~855 nm) of the dye absorbance matches closely with the emission wavelength of micro-VCSELs (Figure 2c), while the emission spectra exhibit the maximum at ~900 nm, which is readily detectable by the silicon photodiode.

To evaluate the sensing characteristics, the integrated sensor assembly was first immersed in a glass bath containing the dye solution, where the epoxy encapsulation effectively prevented the liquid penetration into the underlying devices and metal interconnects. Figure 2d shows IV curves of the detector (i.e., Si-PD) measured at various dye concentrations under a fixed output power (~2 mW) of the light source (i.e., micro-VCSEL). As expected, the output current ($I_{solution}$) of Si-PD in a dye solution systematically increased with the dye concentration owing to the increased level of fluorescent emission. The baseline current ($I_{solvent}$) in the liquid bath was slightly higher than that in the air owing to the reflection of excitation light at the air/liquid interface (see the inset of Figure 2e). The background-normalized PD current ($I_{solution}/I_{solvent}$) at a fixed applied PD voltage (e.g., −1.0 V) linearly increased over nearly 2 orders of magnitude of dye concentration (Figure 2e), where the smallest detectable concentration of luminophore was 2 × 10^{-5} wt %, corresponding to ~270 nM at the $I_{solution}/I_{solvent}$ of ~1.17. The limit of detectable concentration observed in this study is partly due to the weak light absorption of 3 μm thick silicon photodiode, which is expected to improve substantially by employing optically thick photodiodes (e.g., thicker silicon or direct bandgap InGaAs).

To construct large area, opto-fluidic fluorescence sensors in thin, monolithic form factors, a fluidic channel prepared by softlithographic molding of PDMS was directly laminated on top of the printed micro-VCSEL/Si-PD arrays, in which a large-volume (2 × 2 × 2 mm^3) reservoir directly above the sensor area was introduced to provide the increased optical path length of excitation light through the luminescent medium (Figure 3a) and enhancing the detection limit. In the reported design of opto-fluidic sensors, some fraction of the stimulated emission from the VCSEL is reflected at the inner and outer wall of the fluidic channel and directed back to the adjacent Si-PD at a steep incidence angle less than ~12° (determined by geometric configurations, Figures 3a and S5), thereby increasing the background current level of the PD. On the other hand, the fluorescent emission from the luminescent medium is isotropic and likely to have much larger incidence angles. To diminish the undesired photon flux of the reflected excitation light to the detector without degrading the absorption of the dye emission, we incorporated an angle- and wavelength-selective spectral filter based on sputter-deposited multilayers of TiO_2 (n = 2.39 @ 850 nm) and SiO_2 (n = 1.46 @ 850 nm) on top of the SU-8 encapsulation covering the Si-PD (Figure 3a). The multilayer-based spectral filter was designed to have a peak reflectance at ~850 nm at normal incidence with characteristics of a low-pass filter such that the excitation light incident at low angles is strongly reflected while the transmission of fluorescent emission at

DOI: 10.1021/acsphotonics.6b00080
ACS Photonics 2016, 3, 912−918

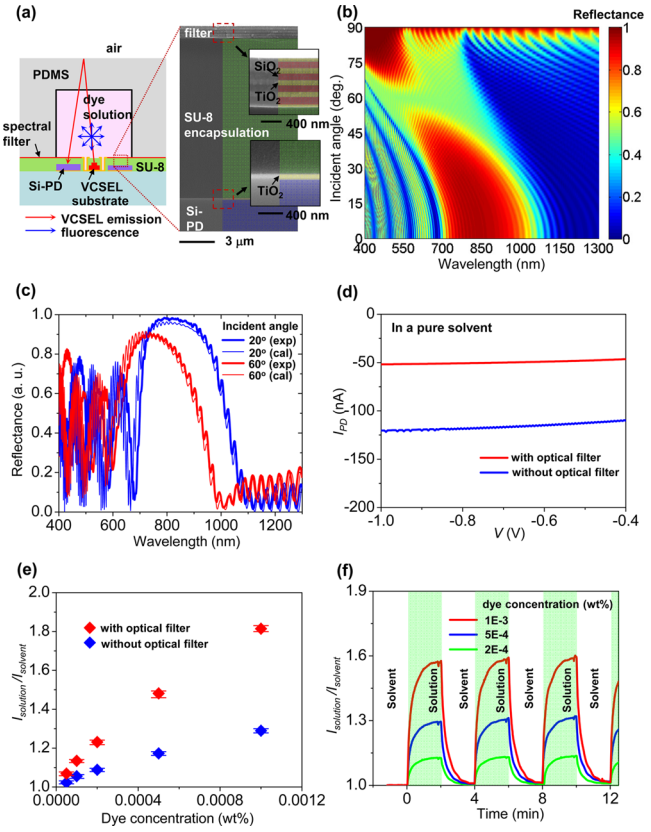

Figure 3. (a) Cross-sectional-view schematic illustration (left panel) of an integrated opto-fluidic sensor based on transfer printed GaAs micro-VCSEL, Si-PD, and PDMS fluidic channel. A cross-sectional SEM image (right panel) corresponding to the dashed box in the schematic shows the detailed structure of the encapsulated Si-PD with spectral filter layers composed of sputter-deposited SiO_2 and TiO_2. (b) Contour plot of calculated reflectance spectra of the spectral filter implemented on the printed Si-PD with a superstrate medium of a dye solution (i.e., dye solution (n = 1.45)-TiO_2 (46 nm)-[SiO_2 (150 nm)-TiO_2 (92 nm)]^3-SiO_2 (150 nm)-TiO_2 (46 nm)-epoxy (14 μm, n = 1.57)-TiO_2 (90 nm)-Si-PD) as a function of wavelength and incidence angle (measured from the surface normal), where the reflectance computed from a transfer matrix method was averaged over transverse electric (TE) and transverse magnetic (TM) polarizations. (c) Measured (thick line) and calculated (thin line) reflectance spectra of the spectral filter in (b) at incidence angles of 20° and 60° averaged over TE and TM polarizations. (d) Baseline (i.e., without dyes) IV curves of a Si-PD in the opto-fluidic fluorescence sensor under a fixed power (2 mW) of the cointegrated micro-VCSEL with and without the spectral filter layers, where a pure solvent without dyes was flown through the fluidic channel. (e) Normalized PD current ($I_{solution}/I_{solvent}$) of the integrated opto-fluidic sensor at various dye concentrations with and without the spectral filter layers. The output optical power and the bias of the micro-VCSEL and the Si-PD were fixed at 2.0 mW and −1.0 V, respectively. The flow rate of the dye solution and solvent was fixed at 13.3 mL/h. (f) Continuous, real-time monitoring of $I_{solution}/I_{solvent}$ as a function of time, where a pure solvent and a dye solution at three different concentrations were alternatingly injected every 2 min at a flow rate of ∼13.3 mL/h to artificially induce a temporal modulation of analyte concentration.

longer wavelengths and high incidence angles is promoted. Figure 3b shows a contour plot of calculated reflectance spectra of the devised spectral filter in a dye solution (i.e., dye solution (n = 1.45)-TiO_2 (46 nm)-[SiO_2 (150 nm)-TiO_2 (92 nm)]^3-SiO_2 (150 nm)-TiO_2 (46 nm)-epoxy (14 μm, n = 1.57)-TiO_2 (90 nm)-Si-PD) as a function of wavelength and incidence angle, where the reflectance value computed from a transfer matrix method was averaged over transverse electric (TE) and transverse magnetic (TM) polarizations.[23,24] The reflectance at 850 nm remained higher than 0.90 up to the incidence angle of ∼27°, suggesting more than 90% of the reflected excitation light can be effectively cut off by the spectral filter. On the other hand, the reflectance at 900 nm is less than 0.20 at incidence angles ranging from 55° to 80°, and less than 0.10 from 60° to 75°, thereby facilitating the absorption of fluorescence emission at large incidence angles. The optimized multilayer structure was fabricated by radio frequency magnetron sputtering of SiO_2 and TiO_2 as shown in the cross-sectional SEM image (Figure 3a). The measured (thick line) reflectance spectra at incidence angles of 20° and 60° averaged over TE and TM polarizations were quantitatively consistent with corresponding calculated reflectance (thin line; Figure 3c). The efficacy of the spectral filter in terms of the sensor performance was first evaluated by monitoring a baseline detector response in a pure solvent (Figure 3d). As expected, the current level of the Si-PD without luminophores substantially decreased by ∼57% after incorporating the spectral filter due to the reduced absorption of the reflected excitation light. The suppressed background current level of the Si-PD led to the enhanced sensor response (i.e., $I_{solution}/I_{solvent}$), which increased, for example, from 1.17 to 1.48 at a dye concentration of 5×10^{-4} wt % without and with the integrated spectral filter, respectively (Figures 3e and S6). The observed detection limit of the opto-fluidic fluorescence sensor was 5×10^{-5} wt %, slightly higher than that obtained from the "in-bath" configuration (Figure 2e) owing to the comparatively smaller optical path length as well as the higher background current. Enabled with the integrated fluidic channel, the reported fluorescence sensor can also accommodate the multiplexed, real-time monitoring of fluorescent analytes. To demonstrate this capability, Figure 3f shows the continuously measured $I_{solution}/I_{solvent}$ as a function of time, where a pure solvent and a dye solution were alternatingly flown through the fluidic channel every 2 min by separate syringe pumps at a flow rate of ∼13.3 mL/h to artificially induce a temporal modulation of the dye concentration. As the dye solution (or a pure solvent) arrived at the "sensing reservoir", the current of Si-PD steeply increased (or decreased) to the saturation (the baseline) level that can be used to quantitatively monitor the amount of analytes in a real time. The transient behavior of the sensor response is attributed to the nonoptimal configuration of liquid delivery system, rather than the intrinsic time resolution of optoelectronic devices, involving a T-shaped connector and a long plastic tubing that can cause unintentional mixing and concentration dispersion (Figure S7a). The detection speed can be further improved with a modified design that can suppress these effects (Figure S7b,c). Although not included in this letter, the reported sensor arrays are also capable of providing spatiotemporal detection over the large area by simultaneously measuring the detector responses from distributed multiple sensors. We also envision the size of device components (especially PDs) can be further reduced for their facile integration with microfluidic systems.

Mechanically flexible fluorescence sensors implemented on a deformable substrate are potentially useful for realizing miniaturized, ultraportable diagnostic systems and wearable/implantable devices for in vivo fluorescence sensing or imaging on freely moving subjects, for which maintaining the device performance and sensor functionality under mechanically deformed conditions is of prime practical importance. To

DOI: 10.1021/acsphotonics.6b00080
ACS Photonics 2016, 3, 912−918

examine this aspect in the reported system, we first measured the performance of individual device components in the integrated fluorescence sensor on a thin (~50 μm) PET substrate in air at various bending radii (Figure 4a). As

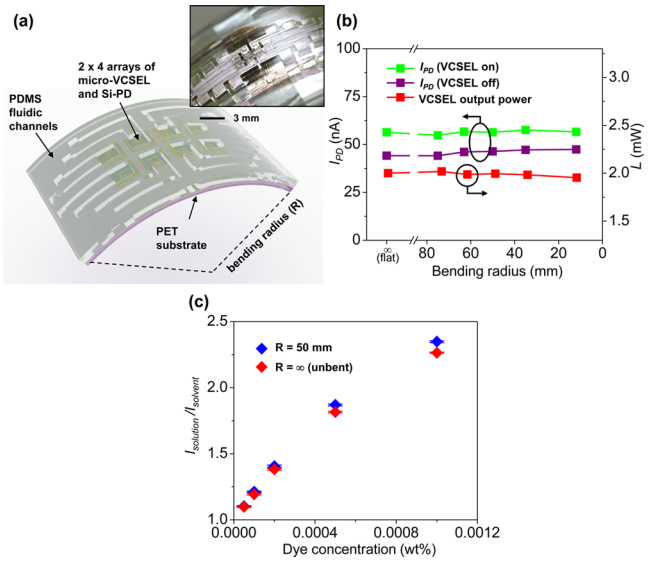

Figure 4. (a) Schematic illustration and photographic image (inset) of flexible opto-fluidic fluorescence sensor on a PET substrate monolithically integrated with a PDMS-based elastomeric fluidic channel. (b) Changes in the output power (L) of the micro-VCSEL, reverse-bias (i.e., −1.0 V) current (I_{PD}) of the Si-PD at "ON" and "OFF" states of the micro-VCSEL as a function of bending radius. (c) Normalized current ($I_{solution}/I_{solvent}$) of the Si-PD in the flexible opto-fluidic sensor, measured in bent (R = 50 mm) and unbent states.

summarized in Figure 4b, the baseline current level of Si-PDs with and without the excitation light as well as the output power of the cointegrated micro-VCSELs, all evaluated without the PDMS fluidic channel, remained invariant at the bending radius of down to ~12 mm owing to the implementation of neutral mechanical plane layout.[15,16] Notably, the mechanically bendable fluorescence sensor integrated with a fluidic channel exhibited comparable detection limit (~5×10^{-5} wt %) to the unbent system at a minimum bending radius (R) of 50 mm (Figures 4c and S8), where the bendability of the system was mainly restricted by the delamination of thick (~2.5 mm) PDMS construct from the substrate.

In summary, we studied materials design and fabrication strategies for mechanically flexible opto-fluidic fluorescence sensors based on 850 nm GaAs micro-VCSELs and Si-PDs on plastics, where transfer printing provided practical pathways to the programmable, scalable assemblies of dissimilar device components into large area sensor arrays on silicon and PET substrates. Metal-coated optical isolation trenches and multilayer-based wavelength- and angle-selective spectral filters effectively reduced the absorption of excitation light arising from the wave-guided spontaneous emission as well as the reflected photons at the wall of the fluidic channels, leading to the enhanced signal-to-noise ratio with the minimum detectable dye concentration of 5×10^{-5} wt %. Liquid-proof construction of printed device assemblies enabled their intimate integration with elastomeric fluidic channels to form large area flexible opto-fluidic sensors on deformable polymeric substrates capable of real-time, continuous monitoring of analyte concentrations as well as operation under mechanically bent conditions. Stretchable forms of sensor arrays based on printed micro-VCSELs cointegrated with high quantum efficiency direct bandgap PDs would be a promising platform for laser-based epidermal physiological diagnostics and therapeutics, where we expect the work presented here will serve as foundation for future research and development.

METHODS

Fabrication of Flexible Integrated Fluorescence Sensors. The fabrication of Si-PD started with the deposition and lithographic patterning of 600 nm-thick Si_xN_y as a selective doping mask by plasma enhanced chemical vapor deposition (PECVD) on a n-type silicon-on-insulator (SOI) wafer (1−10 Ω·cm, Soitec). Thermal diffusion (1000 °C for 15 min under N_2) of p- (BN-1250, Saint Gobain) and n-type (PH-1000N, Saint Gobain) solid-state doping sources defined the heavily doped regions to form pn-junction and ohmic contacts. The C-shaped Si-PDs were delineated by the inductively coupled plasma reactive ion etching (ICP RIE, Plasmalab system 100, Oxford), followed by the partial etching of the SiO_2 sacrificial layer in a concentrated solution of hydrofluoric acid (HF, 49%). Spin-coating of a photoresist (AZ 5214, Clariant) as an anchor and undercut etching of the SiO_2 in HF released the arrays of the Si-PDs from the source wafer for transfer printing onto a silicon or PET substrate using a thin (~1 μm) photocurable adhesive.[15,16,21] Fully functional 850 nm-emitting micro-VCSELs with an aperture area of 22 × 22 μm^2, separately prepared on the GaAs source wafer by the fabrication procedures described elsewhere,[15] were individually printed onto the central region of the C-shaped printed Si-PD on a target substrate using a featured PDMS stamp (350 × 350 × 100 μm^3). The required placement accuracy of transfer printing was in the range of ±10 μm, which was readily achieved using a home-built manual printing stage based on a mask aligner. For VCSELs on a PET substrate, metal layers (Cr/Ag/Au = 15/3000/50 nm) were deposited and patterned by electron-beam evaporation and liftoff to implement a rectangular (700 × 1430 μm^2) heat spreading medium for the overlying micro-VCSEL.[16] Metals (Cr/Au = 30/70 nm) were also incorporated underneath the printed Si-PD to serve as a back-side reflector. After the printing, a single layer (~90 nm) of TiO_2 was deposited on the top surface of the printed Si-PD using a RF magnetron sputtering system (Orion 5, AJA International), followed by patterning of photocurable polymer (SU-8, ~7 μm) and depositing metals (Cr/Ag/Au = 15/1500/50 nm) to form the via holes and optical isolation trenches, and metal interconnects, respectively. Subsequently, an additional polymer layer (i.e., SU-8, ~7 μm) was coated as an encapsulation medium to implement a neutral mechanical plane layout and liquid-proof construction. To suppress the direct absorption of the VCSEL emission to the detector, spectral filter layers based on TiO_2 and SiO_2 were deposited by RF magnetron sputtering on top of the encapsulation layer, where materials deposited on the laser aperture and isolation trenches were removed by wet chemical etching in a diluted HF solution (HF/deionized H_2O = 1:10). The sidewall of the isolation trenches was deposited with metal (Cr, 150 nm) to reduce the wave-guided photon flux from the VCSEL to the detector. The fabrication of the fluorescence sensor arrays were completed by forming external connections using anisotropic conductive film (ACF, Elform) for the electrical control and readout of individual devices. Fluidic channels prepared by softlithographic molding of PDMS using a master via 3D printing (Proto Labs, Inc.)

DOI: 10.1021/acsphotonics.6b00080
ACS Photonics 2016, 3, 912−918

were attached to the completed sensor assembly on a PET substrate. More details of fabrication procedures appear in the Supporting Information.

Electrical, Optical, and Structural Characterization of Integrated Fluorescence Sensors. Electrical properties of micro-VCSELs and Si-PDs were obtained using a semiconductor parameter analyzer (4156C, Agilent Technologies). The output optical power of micro-VCSEL was measured using a calibrated power meter (PD300R, Ophir Optronics), collected through a microscope objective lens (8×, N.A. = 0.15). The reflectance spectra of the spectral filter layers were obtained using an ellipsometer (VASE Ellipsometer, J.A. Woollam Co.), where a silver mirror (Thorlabs Inc.) was used as a 100% calibration standard. The absorbance and emission spectra of the organic dye solution (IR 143, Exciton; dissolved in the mixture of dimethyl sulfoxide (DMSO) and ethylene glycol (EG) (DMSO/EG = 1:2 by weight)) were collected with UV−vis spectrophotometer (Lambda 950, PerkinElmer) and fluorescence spectrophotometer (QM-4, PTI), respectively. The SEM images were taken using a field emission scanning electron microscope (JSM 7001F, JEOL). All measurements of sensing characteristics for the integrated fluorescence sensor were carried out in a light-blocked environment. For the measurement of opto-fluidic sensors, a pure solvent and dye solution were injected sequentially by two syringe pumps (KDS 100, KD Scientific) at a rate of 13.3 mL/h through a long (∼43 cm) tygon tubing (inner diameter is ∼0.89 mm) to a T-junction. A common line (∼15 cm) from the T-junction was then connected to the PDMS fluidic channel (Figure S7).

■ ASSOCIATED CONTENT

Supporting Information

The Supporting Information is available free of charge on the ACS Publications website at DOI: 10.1021/acsphotonics.6b00080.

Figure S1 shows the effect of thermal annealing on the spectral shift of printed micro-VCSELs on a Si wafer. Figure S2 presents the calculated transmittance spectra of the top DBR of micro-VCSELs at various encapsulation layer thicknesses, and schematic illustration of simulated system. Background $I-V$ curves of a printed Si-PD without optical isolation trenches and luminophores are given in Figure S3. Figures S4 and S5 depict cross-sectional schematics of an integrated sensor assembly with optical isolation trenches and an opto-fluidic fluorescence sensor with PDMS-based fluidic channels, respectively. Figures S6 and S8 show $I-V$ curves of a printed Si-PD corresponding to Figures 3e and 4c, respectively. Figure S7 show schematics of liquid delivery system for opto-fluidic sensor measurements and a plot of associated temporal sensor responses (PDF).

■ AUTHOR INFORMATION

Corresponding Author

*E-mail: js.yoon@usc.edu.

Notes

The authors declare no competing financial interest.

■ ACKNOWLEDGMENTS

D.K., B.G., S.-M.L., and J.Y. gratefully acknowledge support from DARPA YFA program under Award No. N66001-12-1-4244. B.T. and N.M. are thankful for the support from the National Science Foundation (CMMI-1068212). The authors thank Donghai Zhu and John Curulli for help in using facilities at Keck Photonics Laboratory and Center for Electron Microscope and Microanalysis (CEMMA) at USC.

■ REFERENCES

(1) Wilson, D. M.; Hoyt, S.; Janata, J.; Booksh, K.; Obando, L. Chemical Sensors for Portable, Handheld Field Instruments. *IEEE Sens. J.* **2001**, *1*, 256−274.
(2) Nolan, E. M.; Lippard, S. J. Tools and tactics for the optical detection of mercuric ion. *Chem. Rev.* **2008**, *108*, 3443−3480.
(3) Drummond, T. G.; Hill, M. G.; Barton, J. K. Electrochemical DNA sensors. *Nat. Biotechnol.* **2003**, *21*, 1192−1199.
(4) Thomas, S. W.; Joly, G. D.; Swager, T. M. Chemical sensors based on amplifying fluorescent conjugated polymers. *Chem. Rev.* **2007**, *107*, 1339−1386.
(5) de Silva, A. P.; Gunaratne, H. Q. N.; Gunnlaugsson, T.; Huxley, A. J. M.; McCoy, C. P.; Rademacher, J. T.; Rice, T. E. Signaling recognition events with fluorescent sensors and switches. *Chem. Rev.* **1997**, *97*, 1515−1566.
(6) Denk, W.; Strickler, J. H.; Webb, W. W. 2-Photon Laser Scanning Fluorescence Microscopy. *Science* **1990**, *248*, 73−76.
(7) Larsson, A. Advances in VCSELs for Communication and Sensing. *IEEE J. Sel. Top. Quantum Electron.* **2011**, *17*, 1552−1567.
(8) Harris, J. S.; sullivan, T. O.; Sarmiento, T.; Lee, M. M.; Vo, S. Emerging applications for vertical cavity surface emitting lasers. *Semicond. Sci. Technol.* **2011**, *26*, 014010.
(9) Thrush, E.; Levi, O.; Cook, L. J.; Deich, J.; Kurtz, A.; Smith, S. J.; Moerner, W. E.; Harris, J. S. Monolithically integrated semiconductor fluorescence sensor for microfluidic applications. *Sens. Actuators, B* **2005**, *105*, 393−399.
(10) Thrush, E.; Levi, O.; Ha, W.; Wang, K.; Smith, S. J.; Harris, J. S. Integrated bio-fluorescence sensor. *J. Chromatogr. A* **2003**, *1013*, 103−110.
(11) O'Sullivan, T.; Munro, E. A.; Parashurama, N.; Conca, C.; Gambhir, S. S.; Harris, J. S.; Levi, O. Implantable semiconductor biosensor for continuous in vivo sensing of far-red fluorescent molecules. *Opt. Express* **2010**, *18*, 12513−12525.
(12) Levi, O.; Lee, T. T.; Lee, M. M.; Smith, S. J.; Harris, J. S. Integrated semiconductor optical sensors for cellular and neural imaging. *Appl. Opt.* **2007**, *46*, 1881−1889.
(13) O'Sullivan, T. D.; Heitz, R. T.; Parashurama, N.; Barkin, D. B.; Wooley, B. A.; Gambhir, S. S.; Harris, J. S.; Levi, O. Real-time, continuous, fluorescence sensing in a freely-moving subject with an implanted hybrid VCSEL/CMOS biosensor. *Biomed. Opt. Express* **2013**, *4*, 1332−1341.
(14) Parashurama, N.; O'Sullivan, T. D.; De La Zerda, A.; El Kalassi, P.; Cho, S.; Liu, H.; Teed, R.; Levy, H.; Rosenberg, J.; Cheng, Z.; Levi, O.; Harris, J. S.; Gambhir, S. S. Continuous sensing of tumor-targeted molecular probes with a vertical cavity surface emitting laser-based biosensor. *J. Biomed. Opt.* **2012**, *17*, 117004−117004.
(15) Kang, D.; Lee, S. M.; Li, Z. W.; Seyedi, A.; O'Brien, J.; Xiao, J. L.; Yoon, J. Compliant, Heterogeneously Integrated GaAs Micro-VCSELs towards Wearable and Implantable Integrated Optoelectronics Platforms. *Adv. Opt. Mater.* **2014**, *2*, 373−381.
(16) Kang, D.; Lee, S.-M.; Kwong, A.; Yoon, J. Dramatically Enhanced Performance of Flexible Micro-VCSELs via Thermally Engineered Heterogeneous Composite Assemblies. *Adv. Opt. Mater.* **2015**, *3*, 1072−1078.
(17) Yoon, J.; Lee, S.-M.; Kang, D.; Meitl, M. A.; Bower, C. A.; Rogers, J. A. Heterogeneously Integrated Optoelectronic Devices Enabled by Micro-Transfer Printing. *Adv. Opt. Mater.* **2015**, *3*, 1313−1335.
(18) Chan, L.; Kang, D.; Lee, S.-M.; Li, W.; Hunter, H.; Yoon, J. Broadband antireflection and absorption enhancement of ultrathin silicon solar microcells enabled with density-graded surface nanostructures. *Appl. Phys. Lett.* **2014**, *104*, 223905.

DOI: 10.1021/acsphotonics.6b00080
ACS Photonics 2016, 3, 912−918

(19) Lee, S. M.; Biswas, R.; Li, W. G.; Kang, D.; Chan, L.; Yoon, J. Printable Nanostructured Silicon Solar Cells for High-Performance, Large-Area Flexible Photovoltaics. *ACS Nano* **2014**, *8*, 10507−10516.
(20) Carlson, A.; Bowen, A. M.; Huang, Y. G.; Nuzzo, R. G.; Rogers, J. A. Transfer Printing Techniques for Materials Assembly and Micro/Nanodevice Fabrication. *Adv. Mater.* **2012**, *24*, 5284−5318.
(21) Kim, T. I.; Kim, M. J.; Jung, Y. H.; Jang, H.; Dagdeviren, C.; Pao, H. A.; Cho, S. J.; Carlson, A.; Yu, K. J.; Ameen, A.; Chung, H. J.; Jin, S. H.; Ma, Z. Q.; Rogers, J. A. Thin Film Receiver Materials for Deterministic Assembly by Transfer Printing. *Chem. Mater.* **2014**, *26*, 3502−3507.
(22) Alias, M. S.; Leisher, P. O.; Choquette, K. D.; Anuar, K.; Siriani, D.; Mitani, S.; Razman, M.; Fatah, A. Electro-opto characteristics of 850 nm oxide-confined vertical-cavity surface-emitting lasers. *ICSE 2006. IEEE Int. Conf. Semicond. Electron., Proc.* **2006**, 227−230.
(23) Hecht, E. *Optics*, 4th ed.; Addison-Wesley: San Francisco, 2002; pp 426−431.
(24) Yoon, J.; Lee, W.; Thomas, E. L. Optically Pumped Surface-Emitting Lasing Using Self-Assembled Block-Copolymer-Distributed Bragg Reflectors. *Nano Lett.* **2006**, *6*, 2211−2214.

DOI: 10.1021/acsphotonics.6b00080
ACS Photonics 2016, 3, 912−918